

# Influence of vortex–vortex interaction on critical currents across low–angle grain boundaries in $\text{YBa}_2\text{Cu}_3\text{O}_{7-\delta}$ thin films

J. Albrecht, S. Leonhardt and H. Kronmüller

*Max-Planck-Institut für Metallforschung, D-70569 Stuttgart, Germany*

(April 26, 2024)

Low–angle grain boundaries with misorientation angles  $\theta < 5^\circ$  in optimally doped thin films of YBCO are investigated by magneto-optical imaging. By using a numerical inversion scheme of Biot–Savart’s law the critical current density across the grain boundary can be determined with a spatial resolution of about  $5 \mu\text{m}$ . Detailed investigation of the spatially resolved flux density and current density data shows that the current density across the boundary varies with varying local flux density. Combining the corresponding flux and current pattern it is found that there exists a universal dependency of the grain boundary current on the local flux density. A change in the local flux density means a variation in the flux line–flux line distance. With this knowledge a model is developed that explains the flux–current relation by means of magnetic vortex–vortex interaction.

The current limiting effect of grain boundaries in high–temperature superconductors (HTSC’s) is a topic of primary importance for the application of these materials. In the last 12 years many measurements have been carried out which show that the transport current across a grain boundary exhibits an exponential decay with increasing misorientation angle  $\phi^{1-5}$ . The reason for this exponential decay is a topic of ongoing discussions and several mechanisms to explain this behavior have been taken into account. At the grain boundary the local distortion of the crystal symmetry causes an array of dislocation cores in the superconducting film. The strain field of these dislocations creates regularly ordered normal conducting regions<sup>6-8</sup>. This leads to a reduction of the effective superconducting interface at the grain boundary and additionally to a reduction of the order parameter in the superconducting regions<sup>9</sup>. This reduction can be explained by a local bending of the electronic band structure<sup>10,11</sup>. A further point of interest is the influence of oxygen deficiency or oxygen disorder which can lead to the appearance of localized states at the grain boundary<sup>12-14</sup>. Considering the pinning scenario of the flux lines located inside the grain boundary it is necessary to remark that the vortices are anisotropic<sup>16,17</sup> which leads to an enhanced coherence length in direction of the boundary and therefore to a reduction of the pinning force density. Most of these effects which lead to the observed exponential decay, however, play just a secondary role if one considers grain boundaries with low misorientation angles in thin films. It can be experimentally found that the exponential decrease of the current density starts above a certain threshold angle of about  $\phi_0 = 5^\circ$  in case of zero field<sup>5,18,19</sup>. The regime of low–angle grain boundaries (LAGB’s) which means in this case grain boundaries with misorientation angles  $\phi < 5^\circ$  can no longer be described by a weak link behavior because the transport current densities which can occur across these grain boundaries can reach the values of the unperturbed film.

In this paper we present local measurements of the critical current density across LAGB’s in thin films per-

formed by a magneto-optical technique. It can be shown that it is not feasible to characterize these grain boundaries only by a global transport current. The critical currents, however, are very sensitive to the local magnetic flux density conditions inside the grain boundary. By applying an appropriate external magnetic field it can be managed that the current limiting role of the grain boundary vanishes. This effect was also found in a similar form in YBCO bulk grain boundaries<sup>15</sup>.

To investigate the role of LAGB’s on the critical current density in superconducting films the following sample geometry is used. YBCO thin films are grown epitaxially on  $\text{SrTiO}_3$  (STO) bicrystalline substrates by pulsed laser deposition. The STO–substrates contain a symmetric  $[001]$  tilt grain boundary with misorientation angles  $\phi < 5^\circ$ . A sketch of the substrate geometry is shown in Fig. 1.

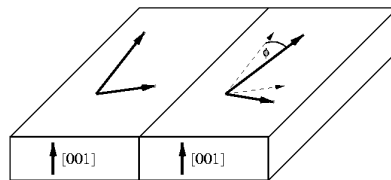


FIG. 1. Sketch of the  $\text{SrTiO}_3$ –substrate geometry. The substrates contain a symmetric  $[001]$  tilt grain boundary with a misorientation angle  $\phi < 5^\circ$ .

The geometry of this grain boundary is adapted from the superconducting film during the growth process. We want to focus in the following on two optimally doped YBCO films with the dimensions of  $1 \text{ mm} \times 1 \text{ mm} \times 300 \text{ nm}$  patterned by chemical etching, which contain a  $2^\circ$  and a  $3^\circ$  grain boundary, respectively.

The measurements that are presented in this paper are performed by applying a magneto-optical technique. As a field sensing layer a ferrimagnetic Lutetium doped Iron garnet film is used which is grown on a Gallium–Gadolinium garnet substrate by liquid–phase epitaxy. This field sensing layer allows the depiction of the magnetic flux density distribution with a spatial resolution of  $3 - 5 \mu\text{m}^2$ . The garnet film is observed by a polarization light microscope and the images are obtained by a charge–coupled device camera with a resolution of  $1000 \times 1000$  picture elements. Due to the fixed magnetic anisotropy of the indicator film a flux density range of about 2 to 150 mT can be observed with high quantitative precision.

In a first measurement a sample with a  $3^\circ$  grain boundary is examined by use of the magneto-optical technique. Fig. 2 shows a grayscale image of the sample after zero–field cooling (ZFC) to 5 K with an afterwards applied field of  $B_{ex} = 48$  mT. Bright parts refer to high magnetic flux densities, black indicates flux–free regions. The image shows  $B_z$ , the flux density component perpendicular to the film.

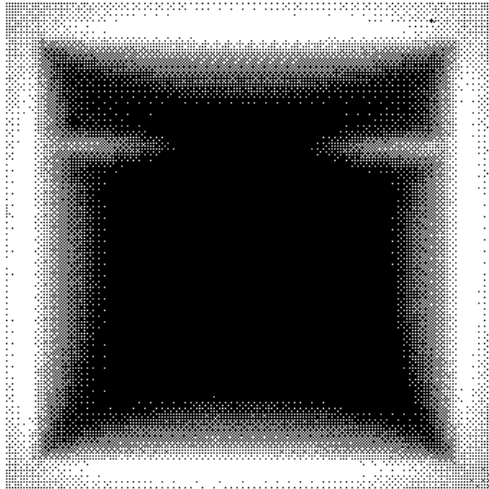


FIG. 2. Grayscale plot of the flux density distribution of a YBCO film with a  $3^\circ$  grain boundary. Bright parts refer to high magnetic flux densities. The image was obtained after zero–field cooling to 5 K with an afterwards applied field of  $B_{ex} = 48$  mT. The sample size is  $1 \times 1 \text{ mm}^2$ .

The gray square represents the region of the superconducting film. Magnetic flux has begun to penetrate the sample in a well–known cushion–like form along the sample’s borders<sup>21</sup>. The influence of the grain boundary can be seen in the two horizontal bright lines in the upper half of the sample. These lines indicate a large penetration of the external flux along the LAGB<sup>23</sup>. This is what can be expected and can be easily understood by a reduced critical current density across the grain boundary, which leads to an enlarged flux penetration in this region. Starting out from the grayscale image in Fig. 2, it can be pointed out that the penetration depth at the grain boundary is about twice as large as in the unperturbed film. That means in a first order approximation a reduced critical current density by a factor of 2 across the LAGB.

In a next step the sample is driven into the fully penetrated state by applying an external magnetic flux density of  $B_{ex} \approx 500$  mT. Afterwards the applied external field is reduced gradually. Fig. 3 shows a series of snapshots at  $B_{ex} = 112$  mT, 96 mT, 80 mT and 48 mT.

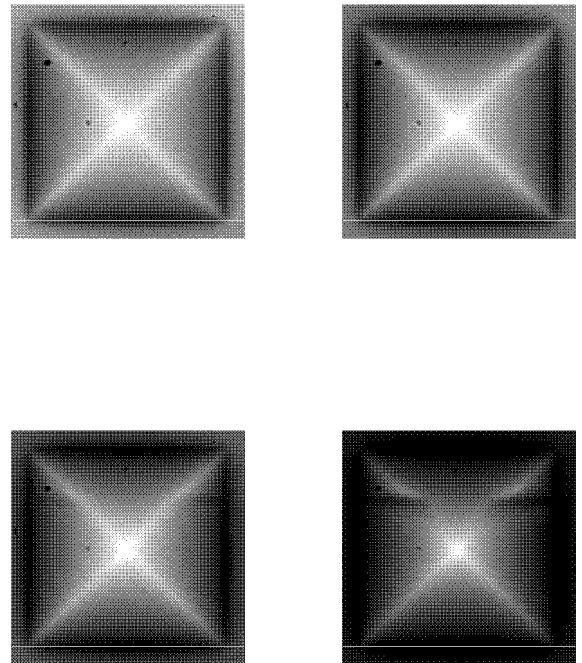


FIG. 3. Magneto-optical images of the flux density distribution of the sample in decreasing magnetic field. After applying an external magnetic flux density of  $B \approx 500$  mT the flux density was gradually reduced. Shown are snapshots at 112 mT (top left), 96 mT (top right), 80 mT (bottom left) and 48 mT (bottom right). The reappearing influence of the grain boundary for decreasing external flux density is clearly visible as the black lines in the upper half of the square.

The behavior of the grain boundary is no longer as trivial to understand as for the ZFC case shown in Fig. 2. For  $B_{ex} = 112$  mT, which is shown in the top left image of Fig. 3 the square-shaped film shows a perfect four-fold symmetry of the flux density distribution. The white discontinuity lines<sup>21</sup> which indicate the trapped flux inside the sample are exactly crossed, no perturbation by the LAGB can be detected. This means that there exists no current limiting effect across the grain boundary; grain boundary and unperturbed film exhibit the same critical current. With decreasing external magnetic field, the grain boundary reappears continuously, the influence of the grain boundary is clearly visible again at  $B_{ex} = 48$  mT. The black lines along the LAGB indicate an expulsion of the trapped magnetic flux due to the collapsing critical currents across the grain boundary. These images prove that the critical current density across a LAGB shows a strong dependence of the magnetic flux density. A similar behavior was found for twin boundaries in YBCO single crystals<sup>24</sup>. The current density increases with increasing flux density up to the value in the unperturbed film, that means that the current limiting effect of an LAGB can be compensated by applying an appropriate magnetic field.

To obtain further information about the current limiting role of LAGB's in thin films it is necessary to determine the critical currents across the grain boundary quantitatively. This is possible by a detailed examination of the magneto-optical data. From the measured perpendicular component of the magnetic flux density  $B_z$  the corresponding current density distribution can be calculated by a numerical inversion of Biot-Savart's law. The relation

$$B_z(x, y) = \mu_0 H_{ex} + \mu_0 \int_V \frac{j_x(\mathbf{r}')(y - y') - j_y(\mathbf{r}')(x - x')}{4\pi |\mathbf{r} - \mathbf{r}'|^3} d^3 r' \quad (1)$$

which is valid for a two-dimensional current density distribution  $\mathbf{j} = (j_x, j_y, 0)$  can be inverted unambiguously by using Fourier transformation and convolution theorem<sup>25</sup>. The lateral resolution of the calculated current density distribution is about 5–7  $\mu m$  and is therefore slightly reduced compared to that of the magnetic field data. This reduction appears because of noise effects in the measurement<sup>25</sup>.

Two different representations of the calculated currents are shown in Fig. 4.

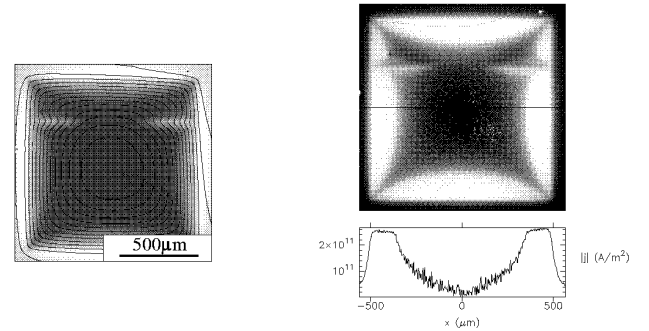


FIG. 4. The current density distribution calculated from the data in Fig. 2. The left image shows an overlay of the flux density distribution and the calculated current stream lines, the right image shows the absolute value of the current density, white parts refer to a high current density.

The left image in Fig. 4 shows an overlay of the flux density distribution known from Fig. 2 and the from these data calculated corresponding current stream lines as solid black lines. The lines which appear outside the sample's region are generated by numerical artefacts in the calculation. The influence of these virtual currents on the current pattern in the superconducting film is very small and thus can be neglected. An important feature of the current density distribution is the strong bending of the stream lines in the region of the grain boundary that can easily be identified by the two bright lines in the upper part of the image. In the right image the absolute value of the current density is plotted as a grayscale. The white color indicates a current density of about  $2.5 \times 10^{11}$  A/m<sup>2</sup>. This representation also shows clearly the perturbing influence of the grain boundary in the upper half of the sample. The small white spots in the center of the sample are artefacts of the numerical calculus. A profile of the absolute values of  $j$  which is taken along the horizontal black line is plotted below. It shows clearly the critical current in the flux-penetrated regions and the screening currents<sup>26</sup> in the center of the sample.

The measured flux density distribution and the corresponding calculated current density distribution are now used to investigate the local relation between field and current. This investigation should clarify the remarkable behavior of the LAGB in the decreasing field shown in Fig. 3. To obtain the local relation between flux and current density we take the spatially resolved data from Fig. 2 and Fig. 4, respectively, and note down the values of flux density and current density for every single picture element. That means for everyone of the about  $1000 \times 1000$  picture elements we get a couple  $(B, j)$  that can be plotted in a  $B$ - $j$  diagram as shown in Fig. 5.

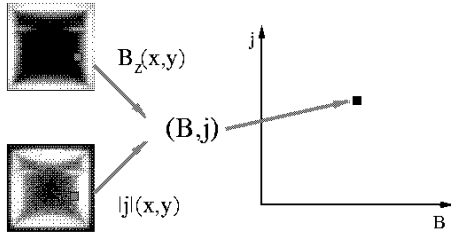


FIG. 5. Sketch of the procedure to obtain the local relation between  $B$  and  $j$ .

This technique was now applied on two different regions of the superconductor. First, of course, on the area of the grain boundary and second, for comparison, on an area of the unperturbed film<sup>23</sup>. As a result we obtain the two curves plotted in Fig. 6.

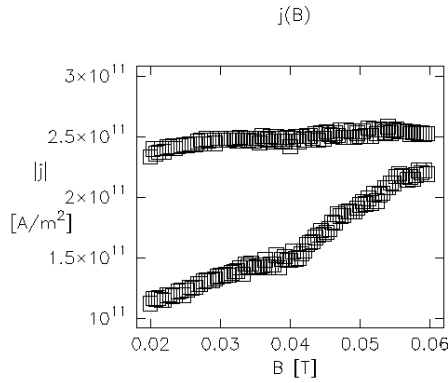


FIG. 6. Relation between the local flux density and the current density. The upper curve refers to the unperturbed film, the lower curve to the LAGB.

The large difference between the two curves is obvious. The upper curve depicts the field dependence of the critical current density in the unperturbed area. It shows a constant value of  $j_c = 2.5 \times 10^{11} \text{ A/m}^2$  over the considered flux density range from 20 to 60 mT. A totally different behavior occurs for the  $B$ - $j$  relation in case of the currents across the grain boundary. A strong increase with increasing flux density can be detected. The exper-

imental data is shown in the lower curve in Fig. 6. The curve has a nearly linear slope with a slight bending at  $B = 40 \text{ mT}$ . This bending is due to local variations in the microstructure of the film and will not be discussed any further. The increasing current density across the grain boundary does not reach the value of the unperturbed film in the considered flux density range, but meets the other curve at  $B \approx 80 \text{ mT}$ . This behavior goes along with the non-perturbing influence of the LAGB in the first image of Fig. 3. Note, that the flux density values of Fig. 3 are valid for the applied external flux density whereas in this case  $B$  is the local magnetic flux density.

Fig. 7 shows the  $B$ - $j$  relation for two grain boundaries with different misorientation angles. The upper curve shows the experimental data for a symmetric  $2^\circ$  grain boundary, the lower curve is again the curve from Fig. 6 for comparison.

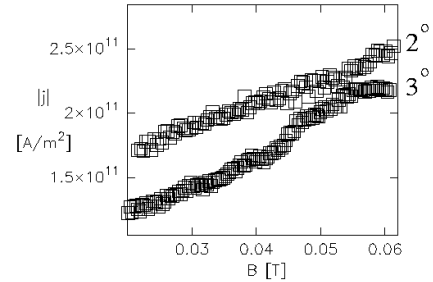


FIG. 7.  $B$ - $j$  curves for a  $2^\circ$  (upper curve) and a  $3^\circ$  grain boundary (lower curve). Both curves show nearly the same slope.

Both of the curves show nearly the same slope, they are just separated by an offset of about  $4 \times 10^{10} \text{ A/m}^2$ , if the small hump of the  $3^\circ$  degree between 50 and 60 mT is neglected. This hump is probably related to a local variation in the microstructure of the sample. Note, that a quantitative comparison of the two measurement makes sense in this case because both films exhibit a field independent critical current density of  $j_c = 2.5 \times 10^{11} \text{ A/m}^2$  in the unperturbed region.

The parallel shape for different angles suggests a universal field dependence of critical currents across LAGB's which can be totally separated from the microstructural properties. The uniform shape of the  $B$ - $j$  relations is an evidence for a additional pinning mechanism of the flux lines which is independent of the microstructural pinning of the grain boundary. Only the local magnetic flux density and thus the flux line-flux line distance originates this effect. As a consequence the critical current can be written as

$$j_c(\phi, B) = j_{c1}(\phi) + j_{c2}(B). \quad (2)$$

In this equation  $j_{c1}(\phi)$  represents the part of the critical current density which is caused by the intrinsic pinning of the grain boundary. This  $j_{c1}$  shows the well known exponential decay with increasing misorientation angle  $\phi$ .  $j_{c2}(B)$  has its origin only in flux line–flux line interaction and is totally independent of the microstructure of the grain boundary. We focus now on the contribution  $j_{c2}(B)$  and try to understand the magnetic field dependency that we observe in our measurements.

To explain the shape of the B–j curve we assume a single vortex located exactly on the LAGB and take a look at the interaction with an Abrikosov flux line lattice in the vicinity of the grain boundary in presence of a Lorentz force. A sketch of the chosen model geometry is shown in Fig. 8. The flux line on the grain boundary is represented as dark gray circle at the top in Fig. 8, the neighboring vortices are presented light gray and white. In the following the force per unit length shall be calculated that is required to drive the vortex along the grain boundary through the nearest neighbors.

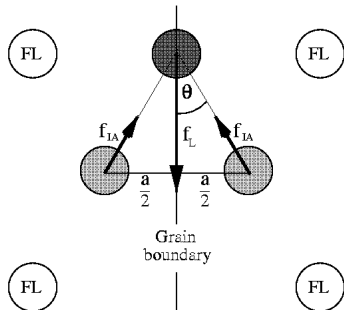


FIG. 8. Sketch of the considered flux line geometry. The dark gray circle represents a flux line located on the grain boundary. The light gray and white circles correspond to the Abrikosov flux line lattice in the vicinity of the grain boundary.

For this calculation numerous assumptions are made which have to be discussed first. The complex flux line–flux line interaction is reduced to magnetic interaction. The distance between two flux lines is several hundred nanometers in the considered flux density range which is at least two orders of magnitude larger than the coherence length. Therefore the flux line core interaction can be neglected in this first order calculation. Also neglected is the anisotropy of the vortex which is located exactly on the LAGB. A flux line on a grain boundary shows a crossover from an isotropic Abrikosov vortex to an extremely anisotropic Josephson vortex with increasing misorientation angle<sup>16</sup>. A certain degree of anisotropy definitely appears in case of the LAGB’s, but the fact that the misorientation angles are very small gives rise

to use isotropic vortices in this model. In addition to this the flux lines in the unperturbed film are assumed to be immobile and only the interaction with the nearest neighbors is concerned. The model neglects any bending effects of the flux lines, e. g. only the two–dimensional projection of the vortices is taken into account.

With all these restrictions the pinning contribution of this model can be calculated. The magnetic interaction force (per unit length) between two vortices is given by deGennes<sup>22</sup>

$$F_{IA} = \frac{\Phi_0^2}{2\pi\lambda^3\mu_0} K_1\left(\frac{a}{\lambda}\right).$$

Here  $\lambda$  is the London penetration depth, which is  $\lambda \approx 150$  nm at  $T = 5$  K,  $\Phi_0$  is the flux quantum,  $a$  the flux line distance and  $K_1$  the modified Bessel function or MacDonald function of first order. The interaction with the two nearest neighbors in Fig. 8 compensates the Lorentz force  $f_L$ , that tries to move the flux line in the LAGB towards the two light gray flux lines. The pinning force of this geometry is now given by the maximum force that appears, if the flux line in the LAGB is forced to pass through the two nearest neighbors

$$F_{pin} = \max_{a,\theta} \left[ 2F_{IA}\left(\frac{a}{\sin\theta}\right) \cos\theta \right],$$

$\theta$  is defined in Fig. 8. To obtain the contribution to the critical current density across the LAGB it is necessary to calculate the current density from the force per unit length. Due to the fact that the magnetic interaction force is present over the whole length of the vortex, one obtains easily  $j_{c2}(a) = F_{pin}(a)/\Phi_0$ , which is the well known definition of a Lorentz force. For better comparison to the experimental data, the dependency on the flux line–flux line distance  $j(a)$  is transformed into a flux density dependence  $j(B)$  using  $B = 2\Phi_0/\sqrt{3}a^2$  for a triangular Abrikosov lattice.

The resulting relation for the interesting flux density range is plotted in Fig. 9.

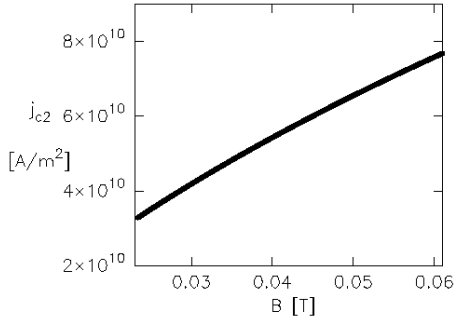


FIG. 9. Contribution of the magnetic vortex–vortex interaction to the critical current density across the grain boundary.

The plot shows a similar increase of the critical current density with increasing flux density as found in the experimental data and the calculation yields current densities of the right order of magnitude.

For an optimal comparison to the measurement the field independent part  $j_{c1}$  of the critical current density of the grain boundary has to be estimated. This can be performed by comparing the data for very low magnetic flux densities where the contribution  $j_{c2}$  is small. Using the data below a local flux density  $B = 30$  mT a value of  $j_{c1} = 1.4 \times 10^{11}$  A/m<sup>2</sup> fits the data best in case of the 2° grain boundary. Plotting now  $j_c = j_{c1} + j_{c2}$  versus the experimental data one obtains Fig. 10.

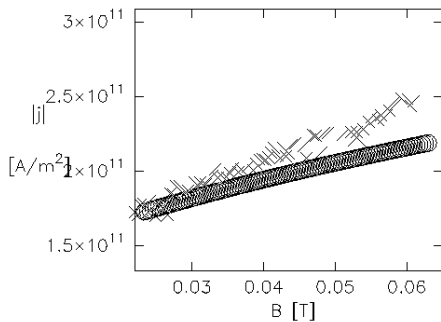


FIG. 10. Comparison of the calculated  $j$ – $B$  relation (circles) with the experimental data (crosses) of the 2° grain boundary.

Both the experimental and the calculated curve show a similar shape. The measured data show a stronger increase than the model predicts but the slope of both curves is in the same range. The largest deviation from the model prediction is found for higher magnetic fields. A possible improvement of the very simple model might be the consideration of more than just nearest–neighbor interaction of the flux lines especially for the higher field range<sup>27</sup>.

To summarize our results, the critical current density across low–angle grain boundaries in thin films of YBCO is investigated by a high–resolution method. The analysis of the local field dependence of the critical current shows a uniform behavior for different misorientation angles. This uniformity can be explained by separating two parts that contribute to the critical current density. One part is correlated to the microstructural properties of the grain boundary and shows the typical drop for increasing misorientation angles. The second part is independent of the microstructure and can be described by vortex–vortex interaction in and in the vicinity of the grain boundary. A model which takes the deGennes magnetic interaction into account is able to reproduce the measured current densities.

The authors are grateful to Ch. Jooss, R. Warthmann and M. V. Indenbom for stimulating and helpful discussions and to G. Cristiani and H.–U. Habermeier for the preparation of the excellent samples.

- 
- <sup>1</sup> D. Dimos, J. Mannhart, P. Chaudhari, and F. K. LeGoues, *Phys. Rev. Lett.* **61**, 219 (1988).
  - <sup>2</sup> M. F. Chisholm and M. F. Pennycook, *Nature* **351**, 47 (1991).
  - <sup>3</sup> R. Gross, in *Interfaces in High-T<sub>c</sub> Superconducting Systems*, edited by S. L. Shinde and D. A. Rudman (Springer-Verlag, New York, 1994), p. 176.
  - <sup>4</sup> A. A. Polyanskii, A. Gurevich, A. E. Pashitskii, N. F. Heinig, R. D. Redwing, J. E. Nordman, and D. C. Larbalestier, *Phys. Rev. B* **53**, 8687 (1996).
  - <sup>5</sup> H. Hilgenkamp, J. Mannhart, and B. Mayer, *Phys. Rev. B* **53**, 14586 (1996).
  - <sup>6</sup> J. B. Hirth and J. Lothe, *Theory of Dislocations* (McGraw–Hill, New York, 1968).
  - <sup>7</sup> A. P. Sutton and R. W. Balluffi, *Interfaces in Crystalline Materials* (Clarendon, Oxford, 1995).
  - <sup>8</sup> J. A. Alarco and E. Olsson, *Phys. Rev. B* **52**, 13625 (1995).
  - <sup>9</sup> A. Gurevich and E. A. Pashitskii, *Phys. Rev. B* **57**, 13878 (1998).
  - <sup>10</sup> J. Mannhart and H. Hilgenkamp, *Supercond. Sci. Technol.* **10**, 880 (1997).
  - <sup>11</sup> H. Hilgenkamp, and J. Mannhart, *Appl. Phys. Lett.* **73**, 265 (1998).
  - <sup>12</sup> R. Gross and B. Mayer, *Physica C* **180**, 235 (1991).

- <sup>13</sup> J. Halbritter, Phys. Rev. B **46**, 14861 (1992).
- <sup>14</sup> B. H. Moeckly, D. K. Lathrop, and R. A. Buhrman, Phys. Rev. B **47**, 400 (1993).
- <sup>15</sup> K. E. Gray, M. B. Field, and D. J. Miller, Phys. Rev. B **58**, 9543 (1998).
- <sup>16</sup> A. Gurevich, Phys. Rev. B **48**, 12857 (1993).
- <sup>17</sup> A. Gurevich and L. D. Cooley, Phys. Rev. B **50**, 13563 (1994).
- <sup>18</sup> Z. G. Ivanov, P. A. Nilsson, D. Winkler, J. A. Alarco, T. Claeson, E. A. Stepantsov, and A. Ya. Tzalenchuk, Appl. Phys. Lett. **59**, 3030 (1991).
- <sup>19</sup> N. F. Heinig, R. D. Redwing, J. E. Nordman, and D. C. Larbalestier, Phys. Rev. B **60**, 1409 (1999).
- <sup>20</sup> L. A. Dorosinskii, M. V. Indenbom, V. A. Nikitenko, Yu. A. Ossip'yan, A. A. Polyanskii, and V. K. Vlasko-Vlasov, Physica C **203**, 149 (1992).
- <sup>21</sup> Th. Schuster, M. V. Indenbom, M. R. Koblischka, H. Kuhn, and H. Kronmüller, Phys. Rev. B **49**, 3443 (1994).
- <sup>22</sup> P. G. de Gennes, Superconductivity of Metals and Alloys, Addison–Wesley (1966).
- <sup>23</sup> J. Albrecht, R. Warthmann, S. Leonhardt, and H. Kronmüller, to be published in Physica C.
- <sup>24</sup> R. Wijngaarden, R. Griessen, J. Fendich, and W.–K. Kwok, Phys. Rev. B **55**, 3268 (1997).
- <sup>25</sup> Ch. Jooss, R. Warthmann, A. Forkl, and H. Kronmüller, Physica **299**, 216 (1998).
- <sup>26</sup> E. H. Brandt, Phys. Rev. Lett. **71**, 2821 (1993).
- <sup>27</sup> J. Pearl, Appl. Phys. Lett. **5**, 65 (1964).